



Cite this: DOI: 10.1039/c6cp06232f

Received 9th September 2016,
Accepted 29th September 2016

DOI: 10.1039/c6cp06232f

www.rsc.org/pccp

An accurate multi-channel multi-reference full-dimensional global potential energy surface for the lowest triplet state of H₂O₂

Jun Li,*^{a,b} Richard Dawes*^c and Hua Guo*^b

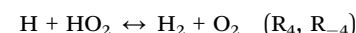
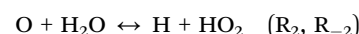
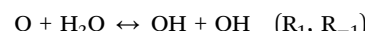
The lowest triplet state of the H₂O₂ system features multiple reaction channels, including several relevant to the combustion of H₂. To accurately map out the global potential energy surface, ~28 000 geometries were sampled over a large configuration space including all important asymptotes, and electronic energies at these points were calculated at the level of the explicitly correlated version of the multi-reference configuration interaction (MRCI-F12) method. A new multi-channel global potential energy surface was constructed by fitting the *ab initio* data set using a permutation invariant polynomial-neural network method, resulting in a total root mean square fitting error of only 6.7 meV (0.15 kcal mol⁻¹). Various kinetics and dynamical properties of several relevant reactions were calculated on the new MRCI potential energy surface, and compared with the available experimental results.

I. Introduction

Due to its prominent role in fundamental combustion kinetics, the H₂/O₂ reactive system has been extensively studied and a number of kinetic models have been reported.^{1,2} In these models, about 20% of the reactions involve low-lying triplet states of the H₂O₂ system. Unlike the ground singlet state of HOOH, which is strongly bound, the triplet states are mostly repulsive in the interaction regions. On the lowest triplet state (1³A'') potential energy surface (PES), there are 12 bimolecular reactions formally possible among the four lowest lying asymptotic channels, namely OH + OH, O + H₂O, H + HO₂, and H₂ + O₂. Some of these reactions are involved in chain branching, propagation, and termination in hydrogen and hydrocarbon combustion.^{1,2} In addition, the hyperthermal reaction of O(³P), which is the dominant species approximately 150 km above Earth's surface, with water vapor produced in spacecraft engines leads to highly excited OH species, which carry unique spectroscopic signatures.³ Because of their importance, rate coefficients have been measured for several of these reactions,^{4–23} and some dynamical studies have also been reported.^{3,24–27}

Ab initio and kinetic studies of this system have been investigated by several theoreticians.^{3,28–35} Among them, Karkach and Osherov presented a comprehensive computational analysis on

the possible transition states on the lowest H₂O₂ triplet state PES,³¹ and showed that the following four reaction channels possess first-order saddle points:



In addition, there also exist O and H exchange channels. As a result, the corresponding multi-channel PES is quite complex and an accurate description of the global potential topography is rather challenging. The first PES of this system was non-reactive, thus incapable of studying these reactions.³⁶

In 2005, Braunstein and co-workers developed the first global reactive PESs for the three lowest lying triplet states of H₂O₂ based on *ab initio* points at a large number of nuclear configurations calculated at the level of the complete active space self-consistent field plus the second-order Møller-Plesset perturbation (CASSCF + MP2) method.^{33,34} These adiabatic PESs were used subsequently in several theoretical studies of kinetics and reaction dynamics.^{33,37,38} However, their 1³A'' PES is only semi-quantitatively accurate as evidenced by its significant underestimation of both the activation and reaction energies for R₁ by 3–4 kcal mol⁻¹, and its large fitting error (3 kcal mol⁻¹ even for low-energy points). To improve the description of the PES, in 2013 we constructed a new analytical

^a School of Chemistry and Chemical Engineering, Chongqing University, Chongqing 401331, China. E-mail: jli15@cqu.edu.cn

^b Department of Chemistry and Chemical Biology, University of New Mexico, Albuquerque, New Mexico 87131, USA. E-mail: hguo@unm.edu

^c Department of Chemistry, Missouri University of Science and Technology, Rolla, Missouri 65409, USA. E-mail: dawesr@mst.edu

PES for the $1^3A''$ state of the H_2O_2 system based on $\sim 36\,000$ points at the level of the unrestricted coupled-cluster singles, doubles and perturbative triples method with an augmented valence triple zeta basis set UCCSD(T)-AE/AVTZ (where “AE” specifies inclusion of all electrons in the correlation treatment),^{39,40} which reproduced the benchmark barrier height³⁵ and experimental reaction endothermicity⁴¹ very well for R_1 . (Note that general geometries on the PESs will have only C_1 point group symmetry, but for convenience in considering some of the product channels, we refer to C_s labels that are applicable to planar geometries.) Kinetic and dynamical studies have been carried out on this PES,^{39,42} as a part of our effort to understand the reaction dynamics of tetra-atomic reactions involving water.⁴³ It should be emphasized that all of these existing PESs cover only the lowest asymptotes, and thus are only suitable for studying R_1 and/or R_2 .

As discussed in previous theoretical studies,^{31–34,39} the electronic structure of the open-shell H_2O_2 triplet system is quite complicated as the low-lying states are close in energy and interact non-adiabatically *via* derivative, Renner-Teller, and spin-orbit couplings. To provide a complete understanding of the kinetics and dynamics of these reactions, coupled PESs of at least the three lowest triplet states are required. Since the CCSD(T) approach can only provide information on the lowest electronic state of a particular spin multiplicity, it is not amenable to the construction of the full PES matrix. Instead, the multi-reference configuration interaction (MRCI) method is favored, particularly for diabatization of the PESs. As a first step in this direction, we focus here on the lowest triplet state ($1^3A''$) of the H_2O_2 system using the MRCI approach, and ignore all non-adiabatic couplings with other states for the time being. Importantly, the new MRCI PES covers higher energies and more dissociation asymptotes than our previous UCCSD(T) PES, thus allowing the study of reactions beyond R_1 and R_{-1} . This publication is organized as follows. The next section (Section II) discusses the *ab initio* calculations, PES fitting, and computational details of the kinetics and dynamical calculations. Section III presents and discusses the results. A summary is given in Section IV.

II. Theory and calculation details

A. Ab initio calculations

The electronic structure of the H_2O_2 triplet system is quite complicated, due to its open-shell nature and non-adiabatic

couplings among several lowest lying electronic states. As a result, multi-reference methods are needed to correctly and accurately map out the PESs and their couplings. Here, we employed the dynamically weighted state-averaged complete active space self-consistent field (DW-SA-CASSCF) method,^{44–46} followed by the explicitly correlated version of multi-reference configuration interaction (MRCI-F12) calculations, which is known to converge quickly with the size of the basis.^{44–48} The nine lowest lying electronic states were included in the CASSCF calculations. As shown in Table 1, the energetics of the system is very sensitive to the electronic structure treatment and basis size. The frozen core (FC) and all electron (AE) calculations were performed with the VTZ-F12 and VQZ-F12, and with the CVTZ-F12 and CVQZ-F12 basis sets of Peterson and co-workers,⁴⁹ respectively. Although the T_1 diagnostic values are sometimes high, suggesting multi-reference character,⁵⁰ we have nonetheless included the CCSD(T)-F12a^{51,52} values at stationary points for comparison (employing the AVDZ and AVTZ basis sets of Dunning and co-workers).^{53,54} After comprehensive testing, as a compromise between accuracy and costs, the MRCI-F12 calculations of the PES points were carried out with the CVDZ-F12 basis set⁴⁹ as implemented in MOLPRO.⁵⁵ A larger basis (CVTZ-F12) was also tested for convergence in single point calculations at the saddle point geometries.

In particular, the electronic energy at a particular geometry was calculated as follows. Following an initial Hartree-Fock calculation, a DW-SA-CASSCF calculation was performed using the full-valence active space (14e,10o) with the 1s electrons of the two oxygen atoms frozen. In order to prevent orbital flipping in the CASSCF calculations, four orbitals (1s and 2s orbitals of the two oxygen atoms) were initially closed and then opened. The maximum weight of the DW-SA-CASSCF scheme was placed on the ground $1^3A''$ state, and weights for excited states were assigned according to their energy differences from the ground state using a sech^2 based energy dependent weight: $\text{sech}^2(\Delta) = [2/(\exp(-\beta\Delta) + \exp(\beta\Delta))]^2$ with Δ being the energy difference from the ground state, and $\beta^{-1} = 3.0$ eV.^{44,45} Dynamic weighting schemes have been shown to provide correct and smooth characterization of the potential energy in regions where multiple excited states are close by.^{44,46,56} A series of iterations were then performed until the energy of the ground electronic state converged within 10^{-6} a.u. (self-consistency),

Table 1 Comparison of the energies (in kcal mol⁻¹ relative to the $O + H_2O$ asymptote) of the stationary points at various levels

Levels	$H_2 + O_2$	$O + H_2O$	$HO + HO$	$H + HO_2$	TS1	TS2	TS3	TS4
FC-3 state-MRCI-F12/Vdz-F12	1.50	0	17.23	57.10	19.31	72.62	72.22	59.69
9-state DW-SA-CASSCF								
FC-3 state-MRCI-F12/VTZ-F12	0.47	0	17.47	56.37	19.66	75.62	71.98	59.05
9-state DW-SA-CASSCF								
AE-3 state-MRCI-F12/CVDZ-F12	3.02	0	18.79	58.57	21.44	74.82	74.66	61.58
9-state DW-SA-CASSCF								
AE-3 state-MRCI-F12/CVTZ-F12	2.00	0	19.05	57.93	21.72	74.48	74.31	60.92
9-state DW-SA-CASSCF								
FC-CCSD(T)-F12a/AVDZ	3.65	0	19.05	57.87	20.66	73.85	72.38	60.04
FC-CCSD(T)-F12a/AVTZ	3.56	0	18.60	58.10	20.88	73.88	72.63	60.45
PIP-NN PES	3.04	0	18.73	58.64	21.67	74.73	74.50	61.83
Expt.	2.44	0	18.03	57.78	—	—	—	—

which resulted in convergence of the subsequent MRCI energy within $\sim 10^{-7}$ a.u.⁵⁷ Internally contracted MRCI calculations^{58,59} were then carried out with the DW-SA-CASSCF wave function as the reference. Note that all electrons were included in the MRCI correlation treatment. The rotated Davidson correction (Q) was included to account for the size extensivity and the higher order excitations approximately.⁶⁰ A three-state MRCI scheme was employed to provide a better description in certain regions with near degeneracy,⁵⁶ and also because we plan to develop PESs for the next two higher triplet states. The three-state MRCI scheme with the rotated reference Davidson correction was employed in all *ab initio* calculations. The rotated reference Davidson correction (Q_{rot}) in MOLPRO has been shown to give better results for multistate calculations, especially in regions of avoided crossings.⁶¹ The above calculation strategy is denoted hereafter as DW-9-state-SA-CASSCF(14e, 10o)/CVTZ-F12 followed by 3-state-AE-MRCI-F12 + Q_{rot} /CVTZ-F12. As shown in Table 1, the results obtained with this method are close to those at the CCSD(T)-F12a level and to the available experimental values at most geometries. We note in passing that the transition states were located on the fitted PES and not separately optimized in MOLPRO at the MRCI level of theory due to the extremely high computational costs.

B. PES fitting

In this work, we focus on the multi-channel PES of the lowest triplet $1^3\text{A}''$ state of the title system, which is largely responsible for all four reactions R₁-R₄, as shown in Fig. 1. In order to provide a globally accurate PES with reasonable computational costs, it is vital to sample the *ab initio* points in the relevant configuration space. In our approach, the stationary points were first surveyed in order to determine the ranges of configurations and energies. Points with energies higher than 180.0 kcal mol⁻¹ relative to the O(³P) + H₂O asymptote were discarded because they are irrelevant to the four reactions. Secondly, an initial set of geometries was generated. In particular, $\sim 12\,000$ points were chosen from our previous $\sim 36\,000$ points

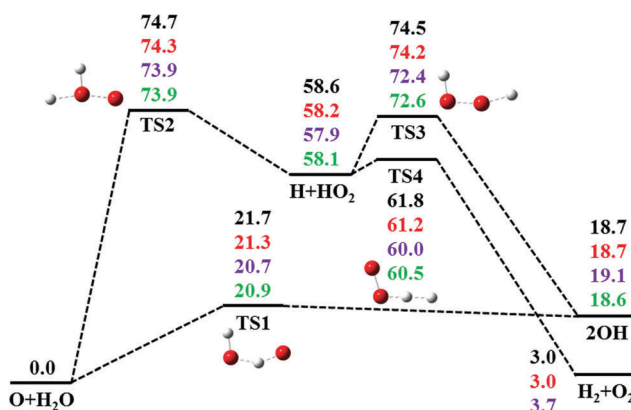


Fig. 1 Schematic illustration of the reaction pathways on the lowest triplet state H₂O₂ PES. All energies are in kcal mol⁻¹ and relative to the O(³P) + H₂O asymptote at various levels: PIP-NN PES, MRCI+Q-F12/CVTZ-F12 PES, CCSD(T)-F12a/AVDZ, and CCSD(T)-F12a/AVTZ, from top to bottom.

used for the 2013 PES of the O + H₂O → OH + OH and H + HO₂ reactions.³⁹ A criterion was used to exclude points that are too close to each other according to the Euclidean distance

$$\chi(\{\vec{r}_i\}) = \sqrt{\sum_i^{n_{\text{bond}}} |\vec{r}_i - \vec{r}'_i|^2}$$

defined in terms of the internuclear distances between two points, $\{\vec{r}_i\}$ and $\{\vec{r}'_i\}$, in the data set. All permutation equivalent points are included in such screenings. Then, these data were used to fit an initial PES. In the next step, classical trajectories with various initial conditions were launched to generate new points in the problematic regions of the PES resulted from lack of data points, such as unphysical holes. New points were then added to patch up these regions if they were sufficiently far from the existing data points according to the Euclidean distance. Some extra points were added in key regions, for instance, in the vicinities around the stationary points and minimum energy paths. This procedure was iterated multiple times until convergence was reached.

The invariance with respect to permutation of identical atoms in the system is an essential feature of the PES. Here, the number of permutation operations is $2! \times 2! = 4$, which can also help reduce the number of points needed in the PES generation. The fitting of the permutationally invariant PES was carried out using the recently proposed permutation invariant polynomial-neural network (PIP-NN) method.^{40,62} This PIP-NN method combines the advantages of both the PIP⁶³ and NN methods,⁶⁴⁻⁶⁷ and has shown its flexibility in representing global full-dimensional PESs for systems with up to 7 atoms.⁶⁸ Explicitly, the six-dimensional (6D) PES was fit using the following functional form, represented by a feed-forward NN with two hidden layers:

$$V = b_1^{(3)} + \sum_{k=1}^K \left(\omega_{1,k}^{(3)} \cdot f_2 \left(b_k^{(2)} + \sum_{j=1}^J \left(\omega_{k,j}^{(2)} \cdot f_1 \left(b_j^{(1)} + \sum_{i=1}^I \omega_{j,i}^{(1)} \cdot G_i \right) \right) \right) \right), \quad (1)$$

where I, J and K are the number of PIPs (G_i) of the input layer, the number of the neurons of the first and second hidden layers, respectively; f_1 and f_2 denote the transfer functions used in the two hidden layers, with their explicit forms being $\tanh(x) = (e^{2x} - 1)/(e^{2x} + 1)$; $\omega_{j,i}^{(l)}$ are the weights that connect the i th neuron of the $(l-1)$ th layer and the j th neuron of the l th layer, and $b_j^{(l)}$ are the biases of the j th neurons of the l th layer. The parameters, namely weights ω and biases b , are determined by non-linear least squares fitting using the Levenberg–Marquardt algorithm.⁶⁹ The major difference between the PIP-NN method and a conventional NN approach is that the permutation invariance is adapted at the level of the input layer of the NN. Other possible inputs (such as coordinates) are replaced by low-order PIPs, namely, symmetrized monomials of Morse-like

variables of internuclear distances,⁷⁰ $\mathbf{G} = \hat{S} \prod_{i < j}^{N} p_{ij}^{l_{ij}}$, $p_{ij} = \exp(-\lambda r_{ij})$ ($\lambda = 1.0 \text{ \AA}^{-1}$, $i, j = 1-4$), and \hat{S} the symmetrization operator which consists of all the permutation operations in the system. In this work, the NN input includes all symmetrized monomials up to the

third degree ($I = 32$), which is necessary to enforce the correct atomic permutation symmetry for A_2B_2 systems.⁴⁰

C. Kinetics

The thermal rate coefficients for all reactions on the H_2O_2 triplet state PES were computed using the canonical variational transition-state theory (CVTST, or CVT).⁷¹ The quantum effects for coordinates perpendicular to the reaction path were included *via* quantum mechanical vibrational partition functions with the harmonic approximation, while the quantum effects in the reaction coordinate were considered using the micro-canonical optimized multidimensional tunneling (μ OMT) approach.⁷¹ The classical rotational partition functions were employed. The rate coefficients were computed on the PIP-NN PES interfaced to POLYRATE.⁷²

D. Dynamics of the O + HOD ($\nu_{OH} = 4$) reaction

Standard QCT calculations were performed using VENUS^{73,74} to simulate the quantum-state resolved experiment: O + HOD ($\nu_{OH} = 4$) → OH + OD at a collision energy of 590 cm^{-1} .²⁶ The trajectories were initialized from a reactant separation of 10.0 \AA , and terminated when the product/reactant species reached a separation of 8.0 \AA . The maximal necessary impact parameter (b_{\max}) was determined using an opacity function estimated by a total of 10^4 trajectories with trial values. The initial vibrational coordinates and momenta of HOD were sampled using the normal mode approach. Other scattering parameters, such as the impact parameter, vibrational phases, and spatial orientation of the initial reactants, were sampled *via* a Monte Carlo approach. The propagation time step was selected to be 0.05 fs , which conserves the total energy very well. A few exceptionally long trajectories were terminated if the propagation time reached a pre-specified value (10.0 ps). The gradient of the PES was calculated numerically by a central-difference algorithm. Almost all trajectories conserved energy to within a chosen condition ($0.001\text{ kcal mol}^{-1}$).

The total reactive integral cross section (ICS) was computed as follows:

$$\sigma_r(E_c) = \pi b_{\max}^2(E_c) P_r(E_c), \quad (2)$$

where the reaction probability at the specified collision energy E_c is given by the ratio between the number of reactive trajectories (N_r) and the total number of trajectories (N_{total}):

$$P_r(E_c) = N_r/N_{\text{total}} \quad (3)$$

with the standard error given by $\Delta = \sqrt{(N_{\text{total}} - N_r)/N_{\text{total}}N_r}$.

The vibrational actions of the two diatomic products were determined semi-classically. The traditional histogram binning (HB) method and Gaussian binning (GB) method⁷⁵ were employed to determine the final state distributions of the products from the trajectories. In the GB method, Gaussian weights are applied in vibrational quantization of both products. As a result, large numbers of trajectories are needed to achieve reasonable statistics.

III. Results and discussion

A. Properties of the PES

The calculated $\sim 28\,000 ab initio$ points were fit using the PIP-NN approach. Due to the non-linear nature of the NN training, each training may produce slightly different results. As a result, many fits were generated in order to find the best ones. In the NN fitting, the data were divided randomly into training (90%), validating (5%), and testing (5%) sets. To avoid false extrapolation due to edge points in the random validating and testing sets, we only accepted fits with similar root mean squared errors

$$\left(\text{RMSEs, defined as } \text{RMSE} = \sqrt{\sum_{i=1}^{N_{\text{data}}} (E_{\text{output}}^i - E_{\text{target}}^i)^2 / N_{\text{data}}} \right)$$

for all three sets. Furthermore, the maximum fitting deviation was also employed in selecting the final PIP-NN PESs.

Different NN architectures with two hidden layers were tested. For each architecture, 100 training calculations were performed and the “early stopping” method⁶⁴ was used to prevent overfitting. The training converged quickly, typically within a few hundred steps. A two-layer NN with 40 neurons in each layer was chosen, resulting in a total of 3001 parameters. The RMSEs for the training/validating/testing/total sets and maximum deviation of the three best PESs are $6.1/14.8/17.7/7.7$ and 291.2 meV , $7.4/17.4/19.5/9.1$ and 256.2 meV , and $7.1/17.7/19.3/8.9$ and 294.5 meV , respectively. The final PIP-NN PES was taken as the average of three best fits (committee approach) to further minimize random errors. The final PES has an overall RMSE of 6.7 meV ($0.15\text{ kcal mol}^{-1}$) and a maximum deviation of 129.7 meV ($3.00\text{ kcal mol}^{-1}$). The fitting errors of all the data points are shown in Fig. 2 as a function of energy, which shows a fairly even distribution of the errors. A Fortran program of the PES is available upon request from one of the authors (JL).

As shown in Fig. 1, the energetics (with the zero defined at the $O(^3P) + H_2O$ asymptote) of the stationary points, including the bimolecular asymptotes and transition states on the new

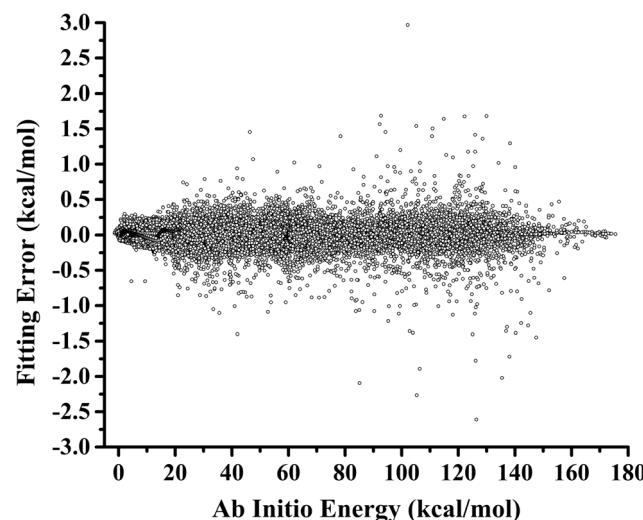


Fig. 2 Fitting errors ($E_{\text{fit}} - E_{\text{ab}}$, in kcal mol^{-1}) as a function of the *ab initio* energy (kcal mol^{-1}) relative to the $O(^3P) + H_2O$ asymptote.

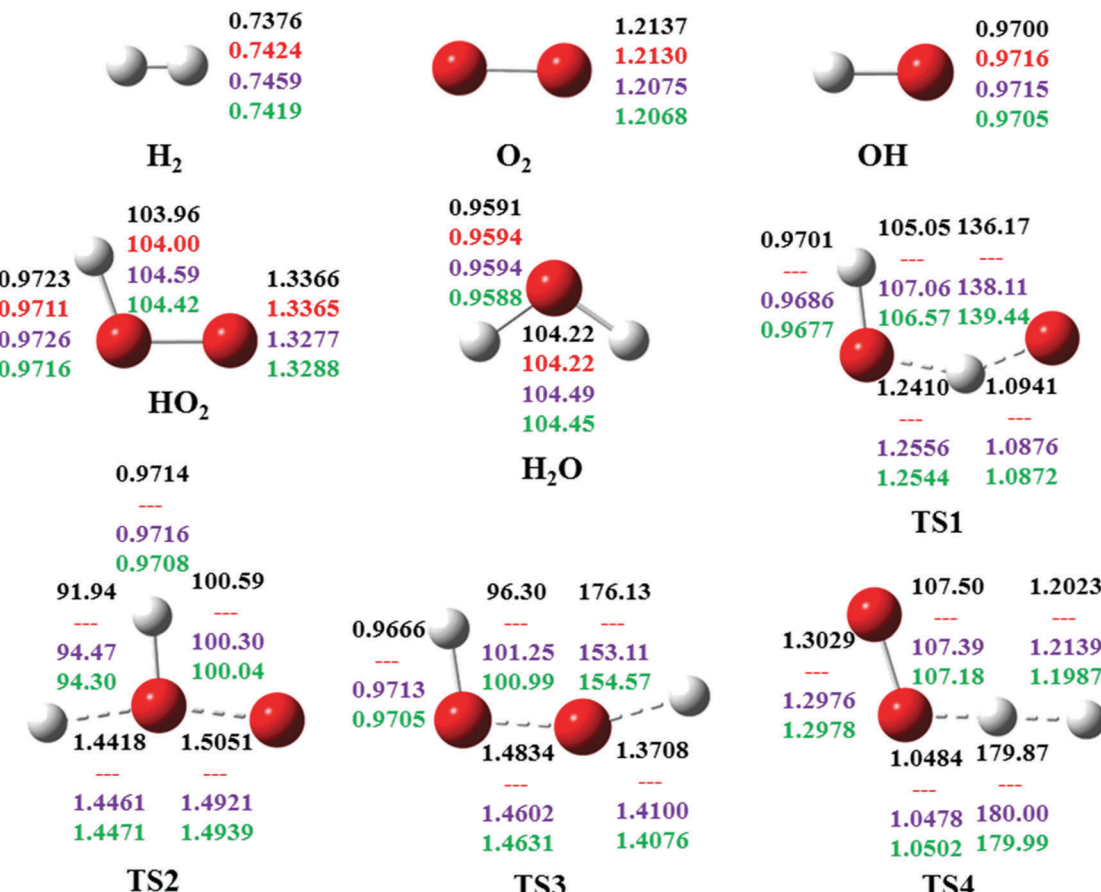


Fig. 3 Optimized geometries (lengths in Å, angles in °) of the reactants, products, and transition states on the lowest triplet state H₂O₂ PES at various levels: PIP-NN PES, MRCI+Q-F12/CVDZ-F12, CCSD(T)-F12a/AVDZ, and CCSD(T)-F12a/AVTZ, from top to bottom.

PIP-NN PES, are similar to those obtained at the levels of UCCSD(T)-F12a/AVDZ, UCCSD(T)-F12a/AVTZ, and 3-state-AE-MRCI + Q_{rot} -F12/CVDZ-F12. However, the energies on the MRCI PES are generally larger than those at the level of UCCSD(T)-F12a, with the largest difference being ~ 2 kcal mol⁻¹ for TS3. While the basis set effect is small for UCCSD(T)-F12a, with the largest difference between AVDZ and AVTZ being 0.45 kcal mol⁻¹ for the OH + OH asymptote, the effects of both the electronic structure theory and the basis set are notable in the MRCI results, indicating the complexity of the electronic structure of the system. Fig. 3 and Table 2 compare the corresponding geometries and frequencies of the asymptotes, and they are similar to each other at different levels of theory. For the transition states, however, the differences are non-negligible. At TS3 ($\text{H} + \text{HO}_2 \leftrightarrow 2\text{OH}$), for example, the forming H-O bond on the MRCI PES is 1.37 Å, 0.04 Å shorter than that at the CCSD(T)-F12a levels, and the breaking O-O bond is 1.48 and 1.46 Å on the MRCI PES and at the CCSD(T)-F12a levels, respectively. In addition, the bond angle OOH is 176.1 and 153.1 degrees on the MRCI PES and at the CCSD(T)-F12a levels, respectively. These differences underscore somewhat dissimilar characters between the MRCI and CCSD(T) PESs in the strongly interacting regions.

On the MRCI PES, the classical energy of the OH + OH asymptote is 18.7 kcal mol⁻¹, which becomes 15.9 kcal mol⁻¹ after correcting the zero-point vibrational energy (ZPVE) and

spin-orbit (SO) splitting.⁷⁶ This is in excellent agreement with the benchmark value, 15.78 kcal mol⁻¹, calculated using the HEAT protocol (with the ZPVE, SO, scalar relativistic and diagonal Born–Oppenheimer corrections) by Nguyen and Stanton,³⁵ and the experimental value of 15.91 ± 0.10 kcal mol⁻¹ derived from the Active Thermochemical Tables (ATcT).⁷⁷ The classical barrier of R₁ (TS1) is 21.7 kcal mol⁻¹ on the MRCI PES, ~ 1 kcal mol⁻¹ higher than that at the CCSD(T)-F12a level, but consistent with our previous result (21.4 kcal mol⁻¹) determined at the UCCSD(T)/CBS level.³⁹ With the ZPVE and SO corrections, it is reduced to 18.7 kcal mol⁻¹, 1.8 kcal mol⁻¹ higher than the value of 16.90 kcal mol⁻¹ obtained with the HEAT protocol.³⁵ This overestimation is likely due to higher excitations not included in the MRCISD theory, and insufficiently recovered through the Davidson correction. TS1 in this system is somewhat analogous to the low barrier (< 2 kcal mol⁻¹) in $\text{F} + \text{H}_2\text{O} \rightarrow \text{HF} + \text{OH}$, which is very sensitive to the treatment of high-order correlation. Here, the converged barrier is much larger, and a slight overestimation should only insignificantly impact the rate coefficients of R₁ at low temperatures, but can affect its reverse R₋₁ more significantly.

The reaction R₂ is only competitive with R₁ at very high temperatures, as its classical reaction endothermicity is quite high, 56–59 kcal mol⁻¹ at levels of MRCI or CCSD(T) as shown

Table 2 Classical energies (E , in kcal mol⁻¹) relative to the asymptote O + H₂O and frequencies (cm⁻¹) of the stationary points on the lowest triplet state H₂O₂ PES

Species	Method	E	Frequencies (cm ⁻¹)					
			1	2	3	4	5	6
O + H ₂ O	PIP-NN PES ^a	0	1660.0	3840.2	3929.3			
	MRCI-F12a ^b	—	1663.6	3847.9	3954.2			
	CCSD(T)-F12a ^c	0	1644.2	3831.1	3940.8			
	CCSD(T)-F12a ^d	0	1646.9	3831.8	3941.7			
H + HO ₂	PIP-NN PES ^a	58.64	1123.0	1449.0	3642.6			
	MRCI-F12a ^b	—	1117.1	1424.5	3685.9			
	CCSD(T)-F12a ^c	57.87	1159.9	1439.5	3645.3			
	CCSD(T)-F12a ^d	58.10	1145.5	1440.3	3656.8			
2OH	PIP-NN PES ^a	18.73	3738.5					
	MRCI-F12a ^b	—	3739.7					
	CCSD(T)-F12a ^c	19.05	3733.7					
	CCSD(T)-F12a ^d	18.60	3738.4					
H ₂ + O ₂	PIP-NN PES ^a	3.05	1531.3	4569.8				
	MRCI-F12a ^b	—	1566.8	4413.8				
	CCSD(T)-F12a ^c	3.65	1608.6	4385.3				
	CCSD(T)-F12a ^d	3.56	1604.9	4401.0				
TS1 O + H ₂ O → 2OH	PIP-NN PES ^a	21.67	-1768.9	393.2	402.3	835.6	1822.1	3743.9
	CCSD(T)-F12a ^c	20.66	-1543.5	317.5	374.3	817.0	1781.5	3780.2
	CCSD(T)-F12a ^d	20.88	-1611.1	369.7	388.6	820.2	1745.6	3784.3
TS2 H + HO ₂ → O + H ₂ O	PIP-NN PES ^a	74.73	-1690.5	466.9	476.9	1041.9	1507.5	3729.7
	CCSD(T)-F12a ^c	73.85	-1723.3	458.3	540.4	950.2	1300.0	3716.8
	CCSD(T)-F12a ^d	73.88	-1717.3	475.8	545.7	946.8	1302.3	3722.9
TS3 H + HO ₂ → 2OH	PIP-NN PES ^a	74.50	-1644.3	267.0	482.9	986.6	1165.5	3822.0
	CCSD(T)-F12a ^c	72.38	-1749.7	424.9	673.9	983.2	1222.6	3710.1
	CCSD(T)-F12a ^d	72.63	-1747.5	410.9	683.5	982.7	1222.9	3717.6
TS4 H + HO ₂ → H ₂ + O ₂	PIP-NN PES ^a	61.83	-2009.1	340.7	641.8	1192.9	1349.9	1627.7
	CCSD(T)-F12a ^c	60.04	-1692.5	322.5	621.7	1197.8	1409.4	1717.7
	CCSD(T)-F12a ^d	60.45	-1759.8	324.1	674.7	1190.3	1400.0	1696.6

^a This work, fitted PIP-NN PES. ^b This work, MRCI+Q-F12/CVDZ-F12. ^c This work, UCCSD(T)-F12a/AVDZ. ^d This work, UCCSD(T)-F12a/AVTZ.

in Table 1. These values are comparable to the previous theoretical value 54.7 kcal mol⁻¹.²⁸ The corresponding value on the MRCI PES is 58.6 kcal mol⁻¹, which is reduced to 54.2 kcal mol⁻¹ with the ZPVE and SO corrections, consistent with the theoretically predicted 53.4 kcal mol⁻¹ at the G3 level, 57.9 kcal mol⁻¹ mol⁻¹ at the AE-CCSD/AVTZ level,³⁰ and the experimental value of 55.3 kcal mol⁻¹.⁷⁶ Its corresponding forward barrier (TS2) is 74.7 kcal mol⁻¹, 0.8 kcal mol⁻¹ higher than that at the CCSD(T)-F12a level and 0.2 kcal mol⁻¹ higher than the previous theoretical value of 74.5 kcal mol⁻¹.²⁸ The ZPVE and SO corrected barrier is 71.8 kcal mol⁻¹, compared to 68.1 kcal mol⁻¹ at G3 or 76.4 kcal mol⁻¹ at AE-CCSD/AVTZ.³⁰

Reactions R₂, R₃ and R₄ are three possible channels starting from the same reactants H + HO₂. Their classical barriers are 16.1, 15.9, and 3.2 kcal mol⁻¹ for TS2, TS3 and TS4, respectively, on the new MRCI PES, suggesting that R₄ is dominant at low temperatures, while R₂ and R₃ become competitive when the temperature is increased. They are consistent with the previous theoretical predictions.^{30,31} The classical energy of the H₂ + O₂ asymptote is 3.0 kcal mol⁻¹, or -1.5 kcal mol⁻¹ with the ZPVE and SO corrections, relative to the O + H₂O asymptote. The latter is consistent with the experimental -1.9 kcal mol⁻¹.⁷⁶ Interestingly, there is no direct reaction path from OH + OH to H₂ + O₂, consistent with the earlier conclusion of Michael *et al.*¹⁵

We have tested the effect of basis size at the stationary points by using MRCI + Q with the larger CVTZ-F12 basis set and the results are given in Table 1. The largest difference is for

H₂ + O₂, where the larger CVTZ-F12 basis result actually slightly overshoots the experimental relative stability by 0.44 kcal mol⁻¹. Using MRCI, it is often difficult to obtain quantitative agreement with experiment for the relative energies of all product channels simultaneously. Often, at least one of the products is well described by a single configuration, yet requires a high-order correlation treatment for an accurate description. As mentioned above, in some cases this can also affect barrier heights. In the F + H₂O → HF + OH reaction, the region of the barrier is well-described by a single configuration, yet is anomalously sensitive to a high-order correlation. In that system the MRCI + Q barrier^{56,78,79} is substantially higher than that obtained at the CCSDT(Q) level.^{56,79–81} Multireference methods are usually required to represent a global PES, but in many cases it remains a challenge to capture a sufficient fraction of the dynamic correlation energy in order to obtain quantitative accuracy at all of the critical points.

Fig. 4–6 show the contour plots of the PIP-NN PES representing two bond lengths involved in reactions R₁, R₃, and R₄, respectively, with all other degrees of freedom optimized. The PESs clearly show the reactant/product asymptotes as well as the transition states. In Fig. 4, the transition state (TS1) is clearly late for the endoergic H + H₂O reaction (see also the TS1 geometry in Fig. 1). The pre- and post-transition state wells are for the van der Waals O–H₂O and hydrogen bonded OH–OH complexes. The latter may facilitate tunneling for the OH + OH reaction.³⁵ The channel with large r_3 and r_2 distances corresponds

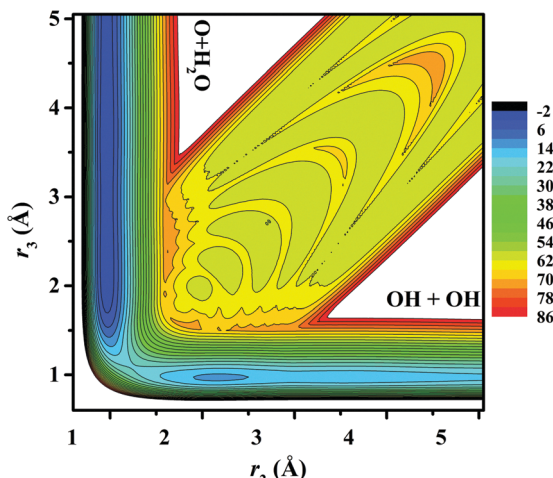


Fig. 4 Contour plot for the $\text{O} + \text{H}_2\text{O} \leftrightarrow \text{OH} + \text{OH}$ reaction along the two reaction coordinates, $\text{O}-\text{H}'$ (r_2) and $\text{H}'-\text{O}'$ (r_3) distances, with the non-reactive $\text{O}-\text{H}$ bond constrained around the equilibrium in H_2O and other internal coordinates optimized. The energies are in kcal mol^{-1} relative to the $\text{O}(^3\text{P}) + \text{H}_2\text{O}$ asymptote and contours are given in -2 – 86 kcal mol^{-1} with an interval of 4 kcal mol^{-1} .

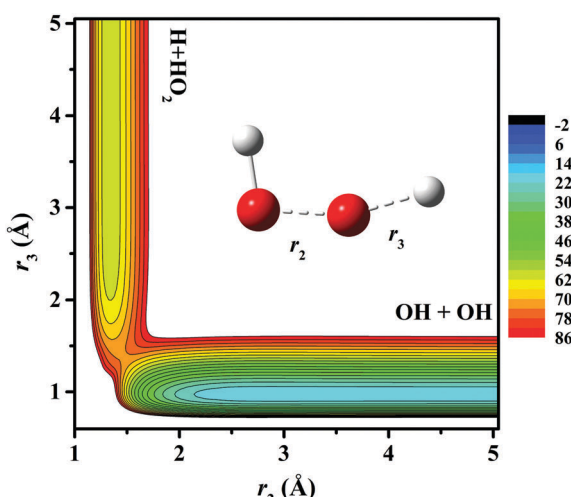


Fig. 5 Contour plot for the $\text{H} + \text{HO}_2 \leftrightarrow \text{OH} + \text{OH}$ reaction along the two reaction coordinates, r_2 and r_3 , as depicted in the inset, with all the other internal coordinates optimized. The energies are in kcal mol^{-1} relative to the $\text{O}(^3\text{P}) + \text{H}_2\text{O}_2$ asymptote and contours are given in -2 – 86 kcal mol^{-1} with an interval of 4 kcal mol^{-1} .

to the $\text{H} + \text{HO}_2$ channel. On the other hand, both transition states (T3 and T4) in Fig. 5 and 6 are manifest early. The $\text{H} + \text{HO}_2$ channel has a very shallow well, while the $\text{OH} + \text{OH}$ channel is dominated by a hydrogen bonded well, clearly shown in Fig. 5. The latter is not apparent because of the coordinates used in plotting the PES.

B. Kinetics

The thermal rate coefficients for all the reactions in both the forward and inverse directions were computed using the CVT/ μ OMT method in POLYRATE. The results are displayed in Fig. 7–10. As shown in Fig. 7, the rate coefficients for R_1

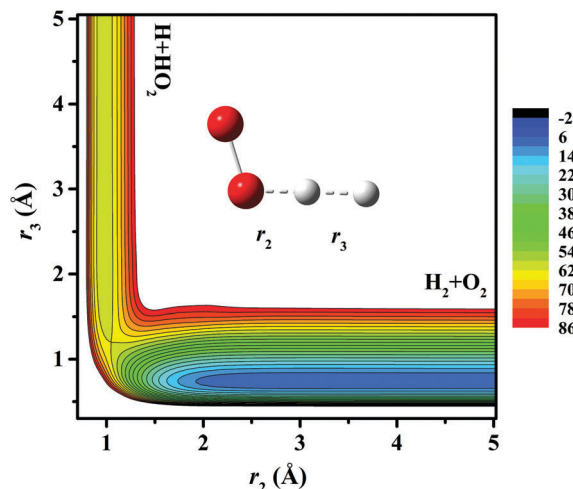


Fig. 6 Contour plot for the $\text{H} + \text{HO}_2 \leftrightarrow \text{H}_2 + \text{O}_2$ reaction along the two reaction coordinates, r_2 and r_3 , as depicted in the inset, with all the other internal coordinates optimized. The energies are in kcal mol^{-1} relative to the $\text{O}(^3\text{P}) + \text{H}_2\text{O}_2$ asymptote and contours are given in -2 – 86 kcal mol^{-1} with an interval of 4 kcal mol^{-1} .

clearly obey the Arrhenius law, but the slight overestimation (see the discussion above) of the TS1 barrier on the MRCI PES leads to underestimation of the rate coefficients of R_1 over the entire temperature range, as expected. The rate coefficients of R_{-1} are much larger, but non-Arrhenius, clearly due to the small barrier and strong tunneling. This hydroxyl self reaction plays an important role in high pressure combustion. Our values are smaller than the existing data, whether from theoretical calculations or measurements.^{13,14,19,21,22,29,31,35} These discrepancies underscore the remaining errors in the MRCI PES, particularly for some of the barriers. It is noted that the transition state barrier on the first excited electronic state PES is 7.5 or 4.8 kcal mol^{-1} higher than TS1 at the level of CASSCF + MP2 or HEAT, respectively. As a result, its contribution to the reaction rate of R_1 is expected

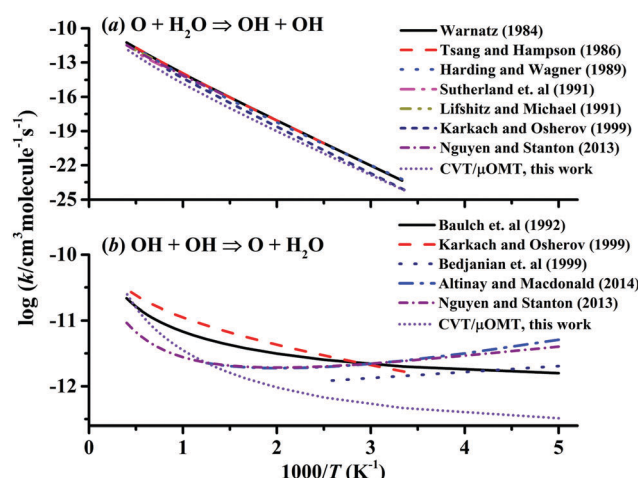


Fig. 7 Plot of the logarithm of the rate constants k ($\text{cm}^3 \text{molecule}^{-1} \text{s}^{-1}$) as a function of $1000/T$ (T is the temperature in K) for the reaction $\text{O} + \text{H}_2\text{O} \leftrightarrow \text{OH} + \text{OH}$: the top and bottom are for the forward and reverse reactions, respectively.

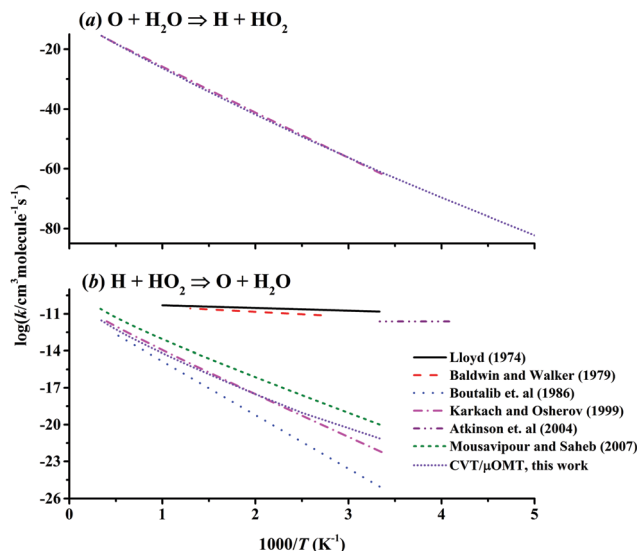


Fig. 8 Plot of the logarithm of the rate constants k ($\text{cm}^3 \text{ molecule}^{-1} \text{ s}^{-1}$) as a function of $1000/T$ for the reaction $\text{O} + \text{H}_2\text{O} \leftrightarrow \text{H} + \text{HO}_2$: the top and bottom are for the forward and reverse reactions, respectively.

to be more significant at high temperatures while its role is negligibly small when the temperature is low.

The rate coefficients of R_2 and R_{-2} are shown in Fig. 8, along with available literature data.^{7,20,23,28,30,31} The temperature dependence of the rate coefficients is clearly Arrhenius, reflecting the significant barriers in both directions. As shown, the CVT/μOMT forward rate coefficients are in excellent agreement with the theoretical predictions by Karkach and Osherov.³¹ For the reverse direction, the CVT/μOMT rate coefficients agree fairly well with those calculated by Boulalib *et al.*,²⁸ Karkach and Osherov,³¹ and Mousavipour and Saheb,³⁰ but are significantly lower than those recommended or estimated by Lloyd, Baldwin and Walker, or Atkinson *et al.*^{7,20,23} It is also clear that the experimental rate coefficients contain large uncertainties for R_{-2} .

The rate coefficients of R_3 and R_{-3} are shown in Fig. 9, along with the available literature data.^{6,9,11,23,30,31} Our CVT/μOMT rate coefficients of R_3 are consistent with the calculations by Karkach and Osherov,³¹ but are significantly lower than those by others, who considered that the reaction occurs *via* the HOOH isomer on the singlet state without a barrier.³⁰ As shown, the calculated reverse results are in excellent agreement with the results of Karkach and Osherov.³¹

The rate coefficients of R_4 and R_{-4} are shown in Fig. 10, along with the available literature data.^{4,6,9,11,12,15,23,30,31} The forward reaction has a relatively small barrier, while the reverse reaction is highly endoergic. As shown, the low-temperature CVT/μOMT rate coefficients of R_4 are significantly smaller than all literature values, although they are with larger uncertainties (e.g., from 3.1×10^{-12} to $7.0 \times 10^{-11} \text{ cm}^3 \text{ molecule}^{-1} \text{ s}^{-1}$ at 300 K). The underestimation is due apparently to the $\sim 1 \text{ kcal mol}^{-1}$ overestimation for the barrier of R_4 at the selected *ab initio* level. For R_{-4} , it can be seen that the current results are consistent with literature values at high temperatures, but apparent

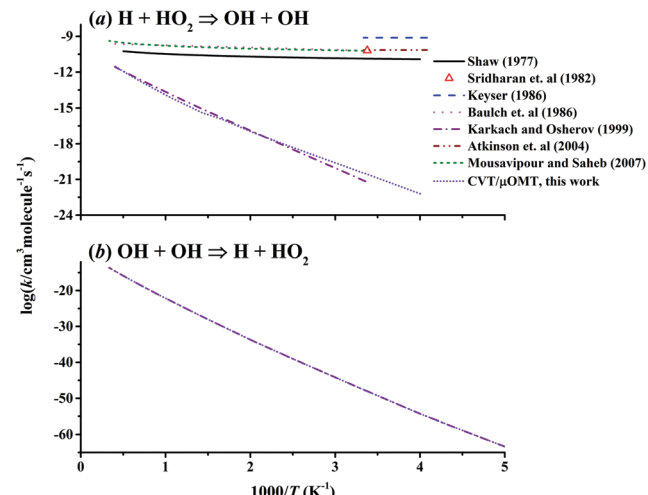


Fig. 9 Plot of the logarithm of the rate constants k ($\text{cm}^3 \text{ molecule}^{-1} \text{ s}^{-1}$) as a function of $1000/T$ for the reaction $\text{H} + \text{HO}_2 \leftrightarrow \text{OH} + \text{OH}$: the top and bottom are for the forward and reverse reactions, respectively.

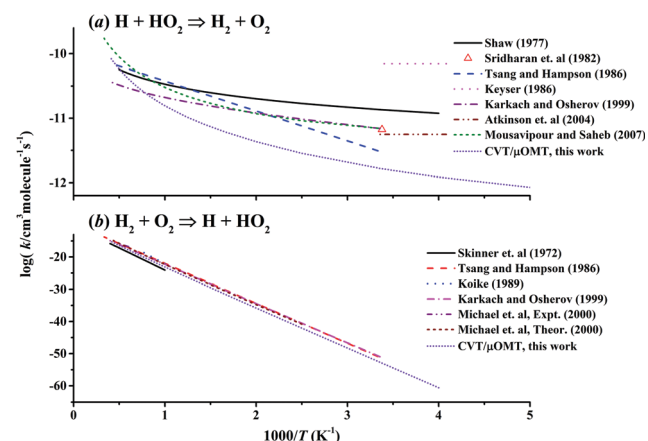


Fig. 10 Plot of the logarithm of the rate constants k ($\text{cm}^3 \text{ molecule}^{-1} \text{ s}^{-1}$) as a function of $1000/T$ for the reaction $\text{H} + \text{HO}_2 \leftrightarrow \text{H}_2 + \text{O}_2$: the top and bottom are for the forward and reverse reactions, respectively.

deviations can be found at low temperatures (note the large scale on the y axis), which again indicates the overestimation of the corresponding barrier height.

C. Dynamics

A total of 500 000 trajectories were calculated to simulate the experiment:²⁶ $\text{O} + \text{HOD}$ ($\nu_{\text{OH}} = 4$) $\rightarrow \text{OH} + \text{OD}$ at a collision energy of 590 cm^{-1} . Despite the fact that the $\text{H}_2 + \text{O}_2$ asymptote is energetically below the $\text{OH} + \text{OH}$ asymptote, no trajectory was found to reach the former. Fig. 11 shows the vibrational populations of the two products OH and OD . One can see that the calculated results resemble the experiment,²⁶ and the GB results are somewhat better than the HB ones, as expected: the OH product is mainly at $\nu_{\text{OH}} = 2$, and the OD product is exclusively in its ground vibrational state ($\nu_{\text{OD}} = 0$). Fig. 12(a) compares the QCT and experimental rotational state distributions of OH ($\nu_{\text{OH}} = 2$). One can see that they are in quantitative

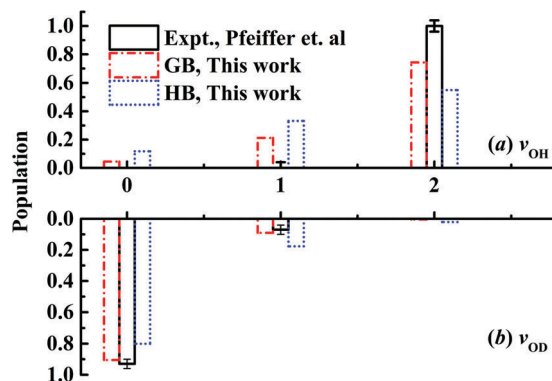


Fig. 11 Normalized QCT vibrational state distributions of the OH and OD products from the reaction $\text{O} + \text{HOD}$ ($\nu_{\text{OH}} = 4$) $\rightarrow \text{OH} + \text{OD}$ and $E_c = 590 \text{ cm}^{-1}$. The available experiment results are adopted from ref. 26.

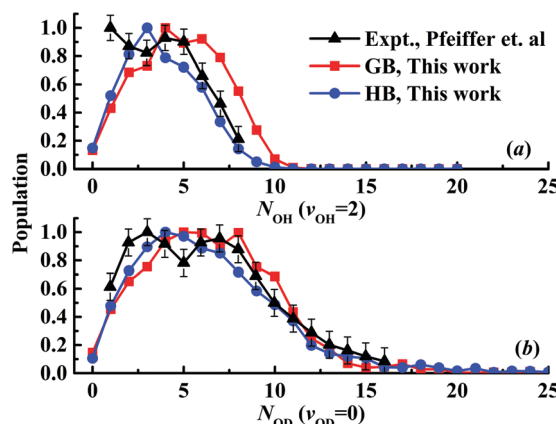


Fig. 12 Normalized QCT rotational quantum state distributions of the product OH for $\nu_{\text{OH}} = 2$ (a) and of the product OD at its vibrational ground state ($\nu_{\text{OD}} = 0$) (b) for the reaction $\text{O} + \text{HOD}$ ($\nu_{\text{OH}} = 4$) $\rightarrow \text{OH} + \text{OD}$ at $E_c = 590 \text{ cm}^{-1}$.

agreement with each other, irrespective of whether HB or GB is employed. The bimodal peaks in the experiment are reproduced in the GB results, thanks to its “quantum mechanical” spirit. Fig. 12(b) displays the rotational state distributions of the OD product ($\nu_{\text{OD}} = 0$). Again, they are similar to each other, with the GB results better reproducing the bimodal peaks in the experiment. The overall agreement with the experimental data provides further evidence that the PES is accurate in its description of these processes.

IV. Summary and conclusions

The development of *ab initio* based global PESs for polyatomic systems has played a key role in recent advances in the understanding of molecular spectroscopy and reaction dynamics.^{43,82,83} These advances have benefitted from the high level electronic structure theory and the advent of various high fidelity fitting techniques.^{46,63,65,68,84,85} Here, we report a global multi-channel PES for the lowest triplet state of the H_2O_2 system based on multi-reference configuration interaction calculations at a large

number of geometries. The *ab initio* data were fit with the high-fidelity PIP-NN method, which rigorously enforces the permutation symmetry in the system. A distinct feature of the new PES is its inclusion of all accessible asymptotes in a wide energy range, thus providing a useful platform for understanding the kinetics and dynamics of a number of combustion related reactions. Dynamical calculations using this PES have reproduced the experimental observations concerning the product state distribution in R_1 . The calculated rate coefficients of the four reactions are in general agreement with experiment, but discrepancies do exist, indicative of remaining errors in the PES. Such small but non-negligible errors are presumably due to the neglect of higher order excitations in the MRCI approach. It is also possible that inclusion of additional coupled excited electronic states will contribute significantly to the calculated rates. Nonetheless, the reported PES represents the most accurate PES for studying the four reactions discussed here and offers a reliable platform for studying a wide range of important reactions, such as the hyperthermal collision of $\text{O}^{(3)\text{P}}$ with water vapor.³ As pointed out earlier, for a complete understanding of these reactions (in particular the details of the dynamics), higher triplet states PESs and non-adiabatic couplings are required. The PES reported here represents the foundation for the future development of the higher triplet state PESs and their couplings.

Acknowledgements

This work was funded by the National Natural Science Foundation of China (21573027 to JL), the US Department of Energy (DE-SC0015997 to HG), and the US National Science Foundation (CHE-1300945 to RD).

References

- M. P. Burke, M. Chaos, Y. G. Ju, F. L. Dryer and S. J. Klippenstein, *Int. J. Chem. Kinet.*, 2012, **44**, 444.
- C. Olm, I. G. Zsély, R. Pálvölgyi, T. Varga, T. Nagy, H. J. Curran and T. Turányi, *Combust. Flame*, 2014, **161**, 2219.
- A. L. Brunsvold, J. Zhang, H. P. Upadhyaya, T. K. Minton, J. P. Camden, J. T. Paci and G. C. Schatz, *J. Phys. Chem. A*, 2007, **111**, 10907.
- G. B. Skinner, A. Lifshitz, K. Scheller and A. Burcat, *J. Chem. Phys.*, 1972, **56**, 3853.
- W. T. Rawlins and W. C. Gardiner, *J. Chem. Phys.*, 1974, **60**, 4676.
- R. Shaw, *Int. J. Chem. Kinet.*, 1977, **9**, 929.
- R. R. Baldwin and R. W. Walker, *J. Chem. Soc., Faraday Trans. 1*, 1979, **75**, 140.
- R. Zellner, *J. Phys. Chem.*, 1979, **83**, 18.
- U. C. Sridharan, L. X. Qiu and F. Kaufman, *J. Phys. Chem.*, 1982, **86**, 4569.
- L. F. Keyser, *J. Phys. Chem.*, 1982, **86**, 3439.
- L. F. Keyser, *J. Phys. Chem.*, 1986, **90**, 2994.
- T. Koike, *Bull. Chem. Soc. Jpn.*, 1989, **62**, 2480.

- 13 A. Lifschitz and J. V. Michael, *Symp. (Int.) Combust., [Proc.]*, 1991, **23**, 59.
- 14 Y. Bedjanian, G. Le Bras and G. Poulet, *J. Phys. Chem. A*, 1999, **103**, 7017.
- 15 J. V. Michael, J. W. Sutherland, L. B. Harding and A. F. Wagner, *Proc. Combust. Inst.*, 2000, **28**, 1471.
- 16 M.-K. Bahng and R. G. MacDonald, *J. Phys. Chem. A*, 2007, **111**, 3850.
- 17 M. Sangwan, E. N. Chesnokov and L. N. Krasnoperov, *J. Phys. Chem. A*, 2012, **116**, 6282.
- 18 M. Sangwan and L. N. Krasnoperov, *J. Phys. Chem. A*, 2012, **116**, 11817.
- 19 G. Altinay and R. G. MacDonald, *J. Phys. Chem. A*, 2013, **118**, 38.
- 20 A. C. Lloyd, *Int. J. Chem. Kinet.*, 1974, **6**, 169.
- 21 W. Tsang and R. F. Hampson, *J. Phys. Chem. Ref. Data*, 1986, **15**, 1087.
- 22 D. L. Baulch, C. J. Cobos, R. A. Cox, C. Esser, P. Frank, T. Just, J. A. Kerr, M. J. Pilling, J. Troe, R. W. Walker and J. Warnatz, *J. Phys. Chem. Ref. Data*, 1992, **21**, 411.
- 23 R. Atkinson, D. L. Baulch, R. A. Cox, J. N. Crowley, R. F. Hampson, R. G. Hynes, M. E. Jenkins, M. J. Rossi and J. Troe, *Atom. Chem. Phys.*, 2004, **4**, 1461.
- 24 O. J. Orient, A. Chutjian and E. Murad, *Phys. Rev. Lett.*, 1990, **65**, 2359.
- 25 D. W. Arnold, C. Xu and D. M. Neumark, *J. Chem. Phys.*, 1995, **102**, 6088.
- 26 J. M. Pfeiffer, E. Woods, R. B. Metz and F. F. Crim, *J. Chem. Phys.*, 2000, **113**, 7982.
- 27 H.-J. Deyerl, T. G. Clements, A. K. Luong and R. E. Continetti, *J. Chem. Phys.*, 2001, **115**, 6931.
- 28 A. Boutilib, H. Cardy, C. Chevaldonnet and M. Chaillet, *Chem. Phys.*, 1986, **110**, 295.
- 29 L. B. Harding and A. F. Wagner, *Symp. (Int.) Combust., [Proc.]*, 1989, **22**, 983.
- 30 S. H. Mousavipour and V. Saheb, *Bull. Chem. Soc. Jpn.*, 2007, **80**, 1901.
- 31 S. P. Karkach and V. I. Osherov, *J. Chem. Phys.*, 1999, **110**, 11918.
- 32 S. Matsika and D. R. Yarkony, *J. Chem. Phys.*, 2002, **117**, 3733.
- 33 M. Braunstein, R. Panfili, P. Shroll and L. Bernstein, *J. Chem. Phys.*, 2005, **122**, 184307.
- 34 P. F. Conforti, M. Braunstein, B. J. Braams and J. M. Bowman, *J. Chem. Phys.*, 2010, **133**, 164312.
- 35 T. L. Nguyen and J. F. Stanton, *J. Phys. Chem. A*, 2013, **117**, 2678.
- 36 M. J. Redmon, G. C. Schatz and B. C. Garrett, *J. Chem. Phys.*, 1986, **84**, 764.
- 37 M. Braunstein and P. F. Conforti, *Chem. Phys. Lett.*, 2012, **523**, 34.
- 38 M. Braunstein and P. F. Conforti, *J. Chem. Phys.*, 2013, **138**, 074303.
- 39 J. Li and H. Guo, *J. Chem. Phys.*, 2013, **138**, 194304.
- 40 J. Li, B. Jiang and H. Guo, *J. Chem. Phys.*, 2013, **139**, 204103.
- 41 B. Ruscic, R. E. Pinzon, M. L. Morton, N. K. Srinivasan, M.-C. Su, J. W. Sutherland and J. V. Michael, *J. Phys. Chem. A*, 2006, **110**, 6592.
- 42 B. Jiang and H. Guo, *J. Am. Chem. Soc.*, 2013, **135**, 15251.
- 43 J. Li, B. Jiang, H. Song, J. Ma, B. Zhao, R. Dawes and H. Guo, *J. Phys. Chem. A*, 2015, **119**, 4667.
- 44 M. P. Deskevich, D. J. Nesbitt and H.-J. Werner, *J. Chem. Phys.*, 2004, **120**, 7281.
- 45 R. Dawes, A. W. Jasper, C. Tao, C. Richmond, C. Mukarukate, S. H. Kable and S. A. Reid, *J. Phys. Chem. Lett.*, 2010, **1**, 641.
- 46 R. Dawes and S. A. Ndengué, *Int. Rev. Phys. Chem.*, 2016, **35**, 441.
- 47 T. Shiozaki, G. Knizia and H.-J. Werner, *J. Chem. Phys.*, 2011, **134**, 034113.
- 48 T. Shiozaki, W. Györffy, P. Celani and H.-J. Werner, *J. Chem. Phys.*, 2011, **135**, 081106.
- 49 J. G. Hill, S. Mazumder and K. A. Peterson, *J. Chem. Phys.*, 2010, **132**, 054108.
- 50 T. J. Lee, *Chem. Phys. Lett.*, 2003, **372**, 362.
- 51 T. B. Adler, G. Knizia and H.-J. Werner, *J. Chem. Phys.*, 2007, **127**, 221106.
- 52 G. Knizia, T. B. Adler and H.-J. Werner, *J. Chem. Phys.*, 2009, **130**, 054104.
- 53 T. H. Dunning, *J. Chem. Phys.*, 1989, **90**, 1007.
- 54 R. A. Kendall, T. H. Dunning and R. J. Harrison, *J. Chem. Phys.*, 1992, **96**, 6796.
- 55 MOLPRO is a package of *ab initio* programs written by H.-J. Werner and P. J. Knowles with contributions from G. Knizia *et al.*
- 56 J. Li, R. Dawes and H. Guo, *J. Chem. Phys.*, 2012, **137**, 094304.
- 57 R. Dawes, P. Lolur, J. Ma and H. Guo, *J. Chem. Phys.*, 2011, **135**, 081102.
- 58 P. J. Knowles and H.-J. Werner, *Chem. Phys. Lett.*, 1988, **145**, 514.
- 59 H.-J. Werner and P. J. Knowles, *J. Chem. Phys.*, 1988, **89**, 5803.
- 60 S. R. Langhoff and E. R. Davidson, *Int. J. Quantum Chem.*, 1974, **8**, 61.
- 61 H. J. Werner, M. Kallay and J. Gauss, *J. Chem. Phys.*, 2008, **128**, 034305.
- 62 B. Jiang and H. Guo, *J. Chem. Phys.*, 2013, **139**, 054112.
- 63 B. J. Braams and J. M. Bowman, *Int. Rev. Phys. Chem.*, 2009, **28**, 577.
- 64 L. M. Raff, R. Komanduri, M. Hagan and S. T. S. Bukkapatnam, *Neural Networks in Chemical Reaction Dynamics*, Oxford University Press, Oxford, 2012.
- 65 S. Manzhos, R. Dawes and T. Carrington, *Int. J. Quantum Chem.*, 2015, **115**, 1012.
- 66 J. Chen, X. Xu, X. Xu and D. H. Zhang, *J. Chem. Phys.*, 2013, **138**, 221104.
- 67 J. Chen, X. Xu, X. Xu and D. H. Zhang, *J. Chem. Phys.*, 2013, **138**, 154301.
- 68 B. Jiang, J. Li and H. Guo, *Int. Rev. Phys. Chem.*, 2016, **35**, 479.
- 69 M. T. Hagan and M. B. Menhaj, *IEEE Trans. Neural Netw.*, 1994, **5**, 989.
- 70 Z. Xie and J. M. Bowman, *J. Chem. Theory Comput.*, 2010, **6**, 26.

- 71 D. G. Truhlar, A. D. Isaacson and B. C. Garrett, in *Theory of Chemical Reaction Dynamics*, ed. M. Bear, CRC, Boca Raton, 1985, p. 65.
- 72 J. C. Corchado, Y.-Y. Chuang, P. L. Fast, W.-P. Hu, Y.-P. Liu, G. C. Lynch, K. A. Nguyen, C. F. Jackels, A. Fernandez Ramos, B. A. Ellingson, B. J. Lynch, J. Zheng, V. S. Melissas, J. Villà, I. Rossi, E. L. Coitiño, J. Pu, T. V. Albu, R. Steckler, B. C. Garrett, A. D. Isaacson and D. G. Truhlar, *POLYRATE*, University of Minnesota, Minneapolis, 2007.
- 73 W. L. Hase, in *Encyclopedia of Computational Chemistry*, ed. N. L. Allinger, Wiley, New York, 1998, vol. 1, p. 399.
- 74 X. Hu, W. L. Hase and T. Pirraglia, *J. Comput. Chem.*, 1991, **12**, 1014.
- 75 L. Bonnet, *Int. Rev. Phys. Chem.*, 2013, **32**, 171.
- 76 NIST Computational Chemistry Comparison and Benchmark Database, NIST Standard Reference Database Number 101, S. Release 17b, ed.: Russell D. Johnson III and <http://cccbdb.nist.gov/>.
- 77 B. Ruscic, R. E. Pinzon, G. von Laszewski, D. Kodeboyina, A. Burcat, D. Leahy, D. Montoya and A. F. Wagner, *J. Phys.: Conf. Ser.*, 2005, **16**, 561.
- 78 J. Li, B. Jiang and H. Guo, *J. Chem. Phys.*, 2013, **138**, 074309.
- 79 T. L. Nguyen, J. Li, R. Dawes, J. F. Stanton and H. Guo, *J. Phys. Chem. A*, 2013, **117**, 8864.
- 80 G. Li, L. Zhou, Q.-S. Li, Y. Xie and H. F. Schaefer III, *Phys. Chem. Chem. Phys.*, 2012, **14**, 10891.
- 81 G. Li, Q.-S. Li, Y. Xie and H. F. Schaefer III, *J. Phys. Chem. A*, 2013, **117**, 11979.
- 82 G. Czakó and J. M. Bowman, *J. Phys. Chem. A*, 2014, **118**, 2839.
- 83 D. H. Zhang and H. Guo, *Annu. Rev. Phys. Chem.*, 2016, **67**, 135.
- 84 M. A. Collins, *Theor. Chem. Acc.*, 2002, **108**, 313.
- 85 M. Majumder, A. S. Ndengue and R. Dawes, *Mol. Phys.*, 2016, **114**, 1.